IEEE Photonics Journal
An IEEE Photonics Society Publication

Open Access

Significantly Enhanced Third Harmonic Generation Using Individual Au Nanorods Coated With Gain Materials

Volume 7, Number 4, August 2015

Jun Song
Jinhong Xian
Hanben Niu
Junle Qu

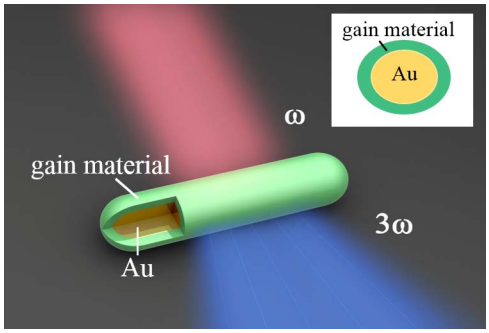

DOI: 10.1109/JPHOT.2015.2449734
1943-0655

IEEE photonics SOCIETY

IEEE

Significantly Enhanced Third Harmonic Generation Using Individual Au Nanorods Coated With Gain Materials

Jun Song, Jinhong Xian, Hanben Niu, and Junle Qu

Institute of Optoelectronics, Key Laboratory of Optoelectronic Devices and Systems of the Ministry of Education/Guangdong Province, Shenzhen University, Shenzhen 518060, China
Key Laboratory of Micro-Nano Measuring and Imaging in Biomedical Optics, College of Optoelectronic Engineering, Shenzhen University, Shenzhen 518060, China

DOI: 10.1109/JPHOT.2015.2449734

Manuscript received May 9, 2015; revised June 17, 2015; accepted June 22, 2015. Date of publication June 24, 2015; date of current version July 3, 2015. Parts of this work were supported by the National Natural Science Foundation of China under Grant 61378091 and Grant 11204226; the National Basic Research Program of China under Grant 2015CB352005 and Grant 2012CB825802; Shenzhen Research Project under Grant ZDSYS20140430164957663 and Grant KQCX20140509172719305; Guangdong Natural Science Foundation under Grant 2014A030312008; the Training Plan of Guangdong Province Outstanding Young Teachers in Higher Education Institutions under Grant Yq2013142; and the Science and Technology Innovation Project of Guangdong Province under Grant 2013KJCX0158. Corresponding author: J. Qu (e-mail: jlqu@szu.edu.cn).

Abstract: We propose a novel design to enhance third harmonic generation (THG) using individual Au nanorods (NRs) coated with gain materials. The present design avoids the use of conventional gap systems, where complicated semiconductor techniques must be used in order to realize the corresponding high-resolution planar structures. As such, this design can contribute to a significant THG enhancement from nanoparticles; this THG is especially favorable for many applications (e.g., photovoltaic devices, bioimaging, and therapy). We perform numerical simulations using a finite-difference time domain (FDTD) in order to identify the origin of the enhanced nonlinear response based on the present system. In addition, we present an effective method to characterize the third harmonics by using Fourier analysis separating them from the excited light. The results show that the THG enhancement of the gain-assisted Au NR with a critical gain coefficient is one to two orders of magnitude greater than the highest values reported for gap THG systems.

Index Terms: Third harmonic generation, Au nanorods, gain materials.

1. Introduction

Localized surface plasmon resonance (LSPR) is obtained by confining the electronic field to a metallic nanoparticle (NP) with size comparable to, or smaller than, the wavelength of the exciting light. The locally enhanced electromagnetic field near the plasmonic nanostructures can be used in various applications ranging from solar cells [1] to bio-probe based imaging [2], surface enhanced Raman scattering (SERS) [3], and cancer therapy [4]. In addition to the enhanced the local electronic field, researchers are currently devoting more attention to optical frequency upconversion based on LSPR, e.g., second harmonic generation [5]–[14], third harmonic generation (THG) [15]–[20], and four-wave mixing [21]–[23]. These optical upconversion effects by using LSPR can be widely applied in various fields. For example, an NP layer with optical

upconversion can be placed at the back of the solar cells to enhance THG by converting some of the near-infrared (NIR) photons to absorbable wavelengths [24]. Moreover, NPs with NIR-excitation and visible emission are well-suited for a number of biomedical applications, owing to their excellent properties. These properties include good penetration depth and low bio-toxicity under long-wavelength excitation [25], and high detectability of optical microscopes and photosensitivity of laser treatments (e.g., photodynamic therapy) in the visible emission range [26].

However, many applications of plasmonics and metamaterials are prone to losses inherent to the interaction of light with metals and hence, the near-field enhancement of individual metallic NPs is insufficient for nonlinear upconversions. Regarded as one of the most effective methods to substantially enhance the LSPR, there is currently significant interest in the construction of various gap systems. These systems are constructed by bringing two or more NPs in close proximity in order to enhance, by several orders of magnitude, the electric field in the hot spot [12], [13], [16], [17]. The generation intensity of the higher order harmonics has also been improved by introducing specific nanostructures with large high-order nonlinear susceptibility into the corresponding gap system [14], [18], [19]. Although highly enhanced upconverting generations have been obtained from these systems, their characteristics are highly dependent on the precision control of the shape and position of each nanostructure in the gap system [27]. As such, these harmonic generation chips must be fabricated via complicated semiconductor techniques, e.g., electron beam lithography. In addition, the planar integrated configuration of optical gap systems is not flexible enough for above photovoltaic and biological applications.

Therefore, the development of metallic nanostructures with both significant near-field enhancement, perhaps comparable to that of a typical gap system, and flexible NP morphology, for achieving a significant enhancement of nonlinear upconversion, remains essential to actual applications.

As an alternative to gap systems, integrating plasmonic nanostructures with gain materials has been proposed as an effective strategy for local field enhancement, which compensates for the loss of conventional LSPR structures [28]. Recently, we proposed a method to significantly enhance the local field of a gap plasmonic system by placing a metallic NP in close proximity to a substrate covered with an $\sim$100 nm film that contains a gain material. Compared with a conventional dielectric substrate, the thin gain film can significantly enhance the local electric fields in the gap between the particle and the substrate; this enhancement, in turn, results in a substantially improved sensitivity of conventional SERS applications [29].

In the present paper, we will demonstrate a novel NP-based nonlinear upconverting design by using an Au nanorod (NR) as a core, which is coated with a gain layer (that acts as a shell). Compared with the planar integrated configuration of optical gap systems, the present NR-based nonlinear upconverting design has more flexible structure so that it is well-suited for various applications including NIR light transformation and activation of solar cells and photodynamic therapy, respectively. Although the present method is equally applicable to other nonlinear processes, the THG is the only example considered in the following discussion. Moreover, we will numerically show that a small gain coefficient in the core-shell NP can induce a significantly better THG compared to that of the conventional Au-NR-based gap system.

2. Simulations and Discussions

As Fig. 1 shows, the proposed nanoparticles consist of an Au NR core (that provides the LSPR) covered with an optically active shell. The dispersion relationship of gold is described by the Johnson-Christy model [30]. The material of the active shell is silica-doped with optical gain inclusions (e.g., organic dyes, rare-earth ions). This structure can be fabricated according to previously published methods [31], [32]. A similar structure has been fabricated through a chemical covalent-bonding method for serving as a plasmonic nanolaser with a spherical gold core [31], or as fluorescence enhancement with Au NRs coated with an Oxazine-725 dye molecule-doped silica shell [32]. In the present paper, we will show that the core-shell nanostructure can be used effectively to enhance nonlinear harmonic generation. Both Au and Ag NPs with various shapes can serve as the LSPR core for the core-shell structure. However, only Au NR will be

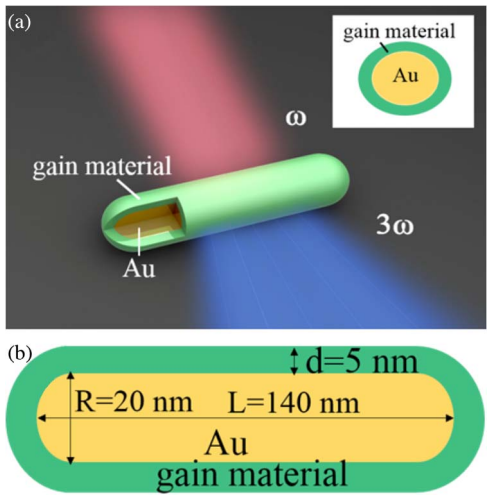

Fig. 1. (a) Schematic and (b) parameter figure of THG from an Au NR (width: R and length: L) coated with gain materials (thickness: d). The inset at the top-right corner of Fig. 1(a) depicts the cross-section of the nanoparticle along the minor axis.

considered as an example in the present paper owing to its tunable absorption peak, which can be moved into the NIR region by increasing the corresponding aspect ratio [33]. Moreover, the Au NR is surrounded by the gain medium that overlaps spatially with the hot-spot of the local plasmonic field and whose gain spectrum overlaps spectrally with the resonant absorption. We set the refractive index of the silica shell to $n - ik$, where the real part (n) has a value of 1.45 and represents the refractive index of the silica, and k defines the level of optical gain. In practice, gain coefficient k can vary depending on the extent of amplification, which corresponds to an amplification coefficient of light intensity as $g = 4\pi k/\lambda$ [34]. The gain material can be made either from dye molecules, semiconductor nanoparticles with sizes of a few nanometers, or from rare earth ions such as Er^{3+}. In general, the gain coefficient is related to both the emission cross section σ_e and the concentration N in these gain systems, which can be written as $g = N\sigma_e$, and the corresponding gain coefficient is given by $k = g\lambda/4\pi = N\sigma_e\lambda/4\pi$. From this formula one can find that the key toward a sufficient large gain coefficient is to have a gain system with a large emission cross section and a high concentration [28]. A gain coefficient on the order of $k = 0.2$ corresponds to an amplification coefficient of light intensity 2.50×10^4/cm for a wavelength of 1003 nm. This amplification coefficient is readily available in this system [28]. The surrounding medium is air.

Based on the system shown in Fig. 1, we performed a steady-state analysis, via finite difference time domain (FDTD) calculations, to determine the effect of the gain coefficient of the outer silica layer on the near- and far-field around the Au NR with gain materials as a shell. Perfectly matched layers (PMLs) were used at the boundaries of the simulation volume in order to prevent non-physical scattering at the boundaries. A mesh size of 1 nm was used in the entire calculation region containing the particle and at the substrate-environment interface, while a smaller (0.2 nm) mesh grid was used around the surface, which has a step refractive index. We chose the following parameters for the system: Au NR width, Au NR length, and thickness of the outer silica layer of 20,140, and 5 nm, respectively. The NP is illustrated under normal incidence with a continuous wave excited light, whose polarization is parallel to the long-axis direction of the Au NR.

Fig. 2(a) shows the plot of the normalized electric field $|E|/|E_0|$ spectra for four different gain coefficients of the outer silica layer, where E is selected as the maximum electric field of the local excited light. The local near-field increases with increasing gain coefficient. In addition, the resonant peak occurs at a wavelength (i.e., the resonant wavelength) of 1003 nm, irrespective

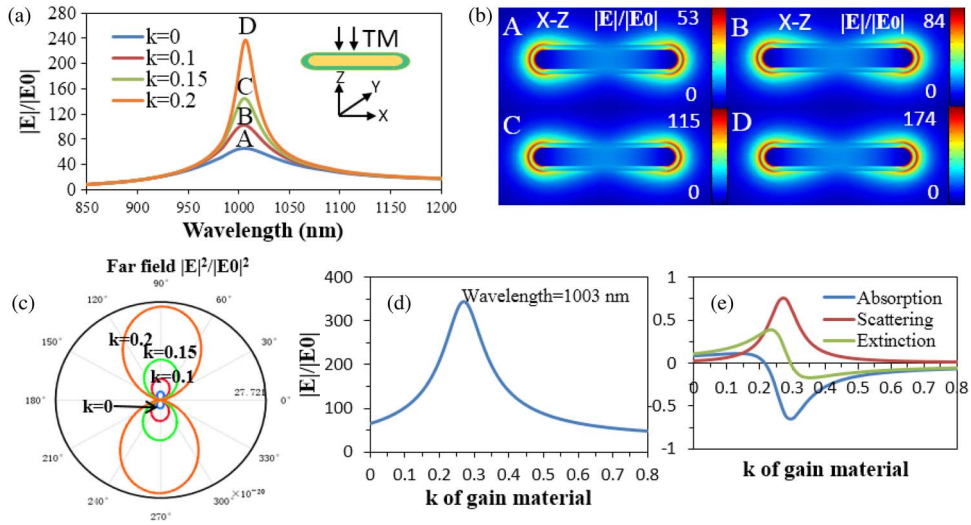

Fig. 2. (a) Plot of the normalized electric field $|E|/|E_0|$ spectra for different gain coefficients of materials encapsulating the Au NR. (b) The electric field distributions at four peak wavelengths, denoted as A, B, C, and D, respectively, in Fig. 2(a). (c) Far-field electric field at various radiation angles for an incident wavelength of 1003 nm. (d) Plot of the normalized electric field $|E|/|E_0|$ and resonant optical scattering, absorption, and extinction cross sections (e) at 1003 nm wavelength as a function of the gain coefficient of the outer silica layer.

of the gain coefficient. Fig. 2(b) shows the near-field distributions at X-Z coordinate plane, at a wavelength of 1003 nm, for four different gain coefficients, denoted as A, B, C, and D in Fig. 2(a). Fig. 2(b) reveals that a gain coefficient of 0.2 results in a field enhancement that is three times larger than that achieved without the gain effect (i.e., $k = 0$); Fig. 2(c) shows the corresponding far-field distributions. The present NR structure can induce a 60° beam divergence. The normalized electric field $|E|/|E_0|$ at a wavelength of 1003 nm [see Fig. 2(d)] also varies with the gain coefficient of the outer silica layer. As the figure shows, the current structure has an optimal gain coefficient ($\sim$0.29), at which the maximal local field enhancement ($\sim$5.3 times stronger than that without gain) can be achieved. In addition, the physical properties in Fig. 2(d) were revealed by calculating the optical spectra of extinction (C_{ext}), scattering (C_{sca}), and absorption (C_{abs}) cross-sections of the considered gain-assisted nanostructures [28]. Similar calculations [Fig. 2(e)] were also performed in this work. The figure exhibits a sharp resonance at the critical point $(k = 0.29)$, where both the scattering and absorption increase rapidly to the peak value and then decrease sharply. The extinction decreases from a large positive value at the critical gain coefficient to a large negative value, a behavior very similar to the familiar phase transition in condensed matter. These features, together with the sharp narrowing of the SPR peak, clearly indicate the induction of lasing at the critical point [28]. When the gain coefficient is smaller than the critical value, a better compensation effect of the scattering loss [see Fig. 2(e)] can be obtained as the gain coefficient increases. However, the lasing phenomenon will occur when the gain coefficient is larger than the critical value, which induces the decrease of the local field intensity of the excited light as the coefficient further increases. Therefore, an optimal THG can be obtained when the gain coefficient equals to the critical value.

Furthermore, we will develop a transient analysis in order to calculate the third harmonics by using a pulse source with a peak power of 1.3 GW/cm^2, 20 fs pulse width, and 1003 nm central wavelength in the FDTD simulation. In previous numerical work, dispersion-less gain coefficients were used to determine the position of the resonant scattering peak [Fig. 2(a)]. Each practical gain material has a corresponding specific gain spectrum. The gain level in the following discussion can be achieved with a Lorentz model when the Lorentz permittivity is negative. In the model, the real and imaginary parts of the refractive index of the gain layer are both

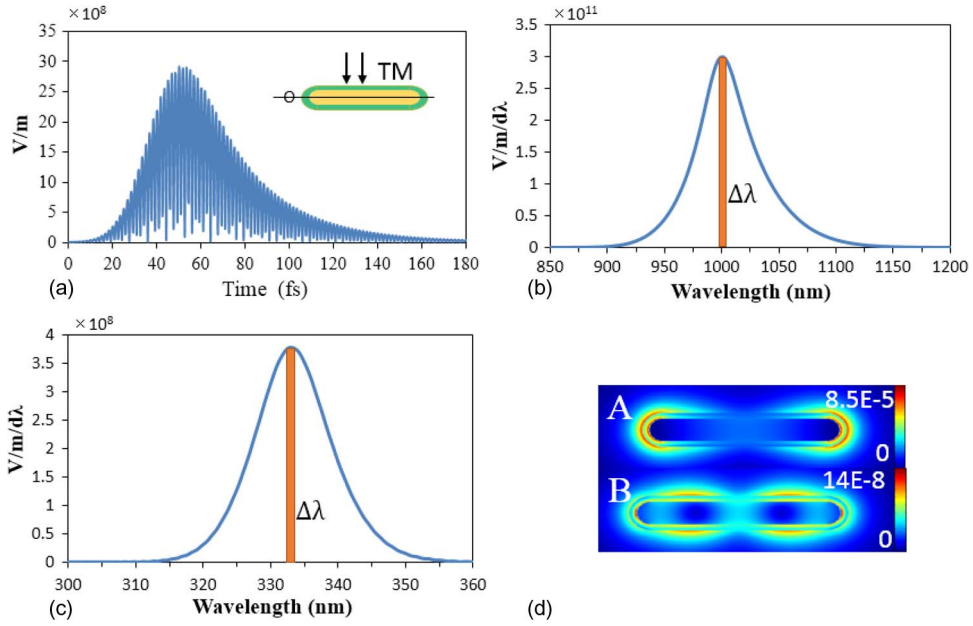

Fig. 3. Extraction principle of the single-frequency excitation light and third harmonic from the total fields based on a Fourier analysis using the proposed Au NR coated with a gain layer ($k = 0.1$) by a pulse source with 1.3 GW/cm^2 peak power, 20 fs pulse width, and 1003 nm central wavelength. (a) The temporal profile of the total electrical fields at a point located 2 nm from the central outer surface. The spectral density of the excitation light (b) and the third harmonics (c) obtained by using the Fourier transformation of the temporal profile. (d) The final near-field distribution of the excitation light and the third harmonics.

dispersive. The gain center frequency is set to the same value as the central wavelength of the Au-NR LSPR, while the width is set to 60 nm (Lorentz linewidth). Under excitation at frequency ω, the third order silica and Au susceptibilities (χ^3) of 6.97×10^{-22} [35] and 7.56×10^{-19} m^2/V^2 [18], respectively, induce a nonlinear polarization $\mathrm{P}^{3\omega} = \varepsilon_0 \chi^{3\omega} \boldsymbol{E}^{\omega} \boldsymbol{E}^{\omega} \boldsymbol{E}^{\omega}$, where ε_0 is the permittivity of free space, and $\boldsymbol{E}^{\omega}$ is the incident electric field at frequency ω. Using the FDTD simulation, we obtained the final near-field distribution including resonant scattering field at frequency ω and the third harmonics at frequency 3ω. When we illuminate a nano-system with a pulse light, we can easily obtain the total fields at any point in the calculation region, as shown in Fig. 3(a). The linear component and the nonlinear harmonics must be separated from the total fields in order to calculate the conversion efficiency of the harmonics. For this purpose, we propose an effective method based on a Fourier analysis. As shown in Fig. 3(b) and (c), we can obtain the function of the spectral density for both the excitation light and the third harmonics by performing a Fourier transformation of the temporal signal in Fig. 3(a). To obtain the final single-frequency intensity, we used ideas, which are based on the basic concept of an integral. As Fig. 3(b) and (c) show, we can discretize the distribution of the spectral density into a linear superposition of countless sufficiently narrow rectangles. In our simulation, each rectangle has a width of 10^{-16} nm and is assumed to be monochromatic. Then, we can obtain the intensity of the electric fields at any reference point for both the excitation light (1003 nm) and the third harmonics (334.33 nm). If we perform the calculation at each point, we can obtain the total near-field distribution of the excitation light and harmonics, as shown in Fig. 3(d).

We used Fourier analysis to separate the third harmonics from the excited scattering light. Fig. 4 shows the final near- and far-field distributions of the third harmonic (with 334.33 nm wavelength) for four different gain coefficients. The critical gain coefficient (i.e., 0.29) in the local near-field distribution can lead to an ~15-time electric field enhancement of the third harmonics compared to that without the gain outer layer. Moreover, an ~239.3 times stronger intensity of

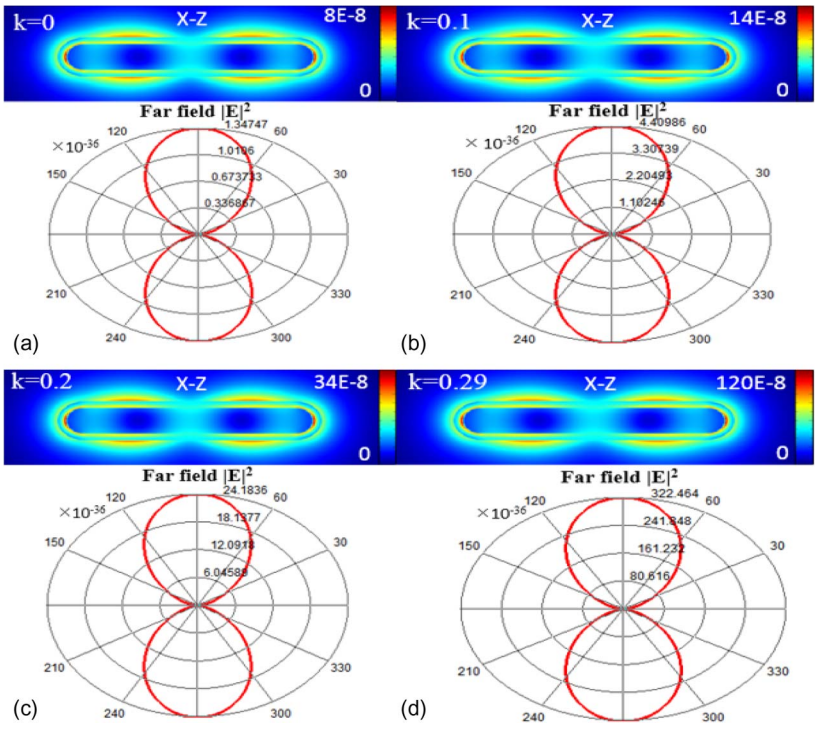

Fig. 4. Near- and far-field distributions of the third harmonic (with 334.33 nm wavelength) for gain coefficients of (a) 0, (b) 0.1, (c) 0.2, and (d) 0.29.

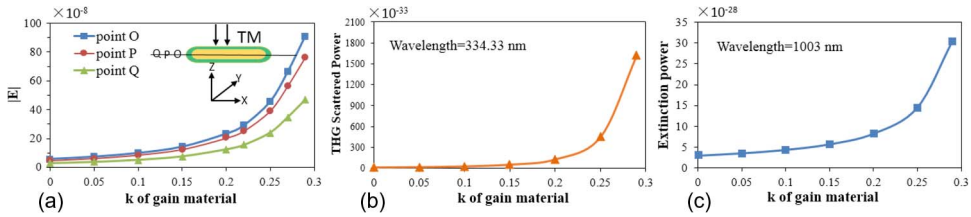

Fig. 5. (a) Local electric field as a function of the gain coefficient for points located 2, 4, and 6 nm, respectively, from the center of the surface of the nanoparticle. (b) THG scattering power (at 334.33 nm) calculated by integrating the THG field around the whole envelop of the NP at different gain coefficients. (c) Extinction power of the excited light plotted as a function of the gain coefficient.

the THG can be obtained from the far-field calculation compared to that of a non-gained nanoparticle. The far-field distribution of the THG also indicates that the THG has the same beam divergence as the scattering excited light. Although the THG directly comes from the strongly enhanced electric field of the excitation light in the gain-assisted nanorod systems, one can see that the maximum areas in the electric field distributions at the THG wavelength (see Fig. 4) are not correlated with those at the fundamental excitation wavelength [see Fig. 2(b)]. This is because the THG wavelength is far away from the plasmonic resonant wavelength of the Au NR [see Fig. 2(a)] so that the mode distribution is entirely different from that at the central resonant wavelength, i.e., the fundamental excitation wavelength.

We characterized the position difference of the THG near-field distribution [see Fig. 5(a)] by selecting three reference points located at distances of 2, 4, and 6 nm, respectively, from the center of the surface of the nanoparticle. The intensity difference between two adjacent points increases with decreasing distance from the critical gain coefficient. In addition, we calculated

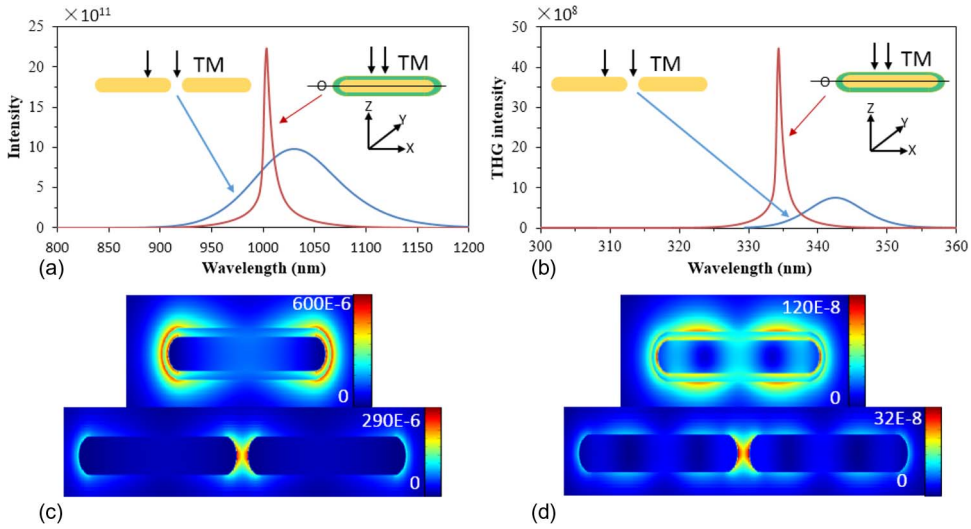

Fig. 6. THG comparison using the current individual Au NR coated with gain materials ($k = 0.29$) and the conventional gap system consisting of two 5 nm-spaced Au NRs. Comparison of the (a) local electric field of the excited light (1003 nm 1028 nm) at the center point of the gap for the gap system and at a point located 2 nm away from the center of the surface of the single nanoparticle system. (b) Generated third harmonic (334.33 nm and 342.67) at the same observation point as Fig. 6(a) for two THG systems. (c) Near-field distributions of the excited light (1003 nm and 1028 nm) for two THG systems. (d) Near-field distributions of the third harmonic (334.33 nm and 342.67 nm) for two THG systems.

the THG scattering power (at 334.33 nm) as a function of the gain coefficient, as shown in Fig. 5(b), by integrating the THG near-field around the whole envelop of the NP. The THG intensity increases significantly, with an exponential-type trend, for gain coefficients close to the critical value. In fact, the THG power at the critical value is ~239.7 times higher than that without any gain coefficient in the silica layer. The local extinction field of the excited light [see Fig. 5(c)] exhibits a similar trend. As previously discussed, we can achieve the optimal THG when the gain coefficient equals to the critical value (i.e., 0.29). In other words, the intensity of both local excited light and THG emission will decrease as the gain coefficient further increases [see Fig. 2(d)]. Therefore, a fundamental excitation at 1003 nm can contribute to the instantaneous third-harmonic response centered at 334.33 nm. Due to the gain compensation, there only is a slight difference of the response speed between the two curves.

A THG gap system composed of two 5 nm-spaced Au NRs was also compared to the core-shell system. The width and length of the two Au NRs are the same as the aforementioned gain-assisted Au NR with the central resonant wavelength at 1003 nm. However, when a gap system with a 5 nm interval between the two Au NRs is formed, the plasmonic resonant wavelength will shift to 1028 nm [see Fig. 6(a)]. Fig. 6(a) shows the comparison of the local electric field of the excited light at the center point of the gap for the double Au-NR system, and at a point located 2 nm from the center of the surface of the single NR system, where the gain coefficient is 0.29. Note that only optimal coefficient is considered in the comparison shown in Fig. 6. One can find the exact THG values with other two non-optimal gain coefficients (i.e., $k = 0.1$ and 0.2) from Fig. 4. In a typical gap system, the intensity of the local near-field increases exponentially with decreasing size of the gap. However, the realizable gap size is limited to the resolution of the easily achievable lateral feature sizes of standard semiconductor techniques, e.g., focused ion beam and photo resist-based electron beam lithography. Therefore, the size of the gap typically exceeds 10 nm [36]. Fig. 6(a) reveals that an approximately three times higher ratio of peak intensity can be obtained between two reference points based on two different systems. Fig. 6(b) shows the comparison of generated third harmonic (334.33 nm wavelength for gap system and 342.67 nm wavelength for core-shell system) at the same observation points

as Fig. 6(a). Based on the present gain-assisted Au-NR design, the peak intensity of the THG is approximately 5.87 times higher than that based on the gap system from the double Au NRs. Fig. 6(c) and (d) compare the near-field distributions of the excited light at respective central resonant wavelength and the corresponding third harmonic, respectively, for the two THG systems. These figures reveal that the THG that uses our design is far superior to that of the conventional gap systems. Although the electric field intensity in the core-shell structure is approximately a factor of 3 higher than that in the gap structure, it is worth noting that the final THG intensity ratio (only 5.87) is far lower than the predicting ratio simply from the equation E^3 (i.e., 27). This is because the medium around the hot spots (i.e., the maximal field distribution) is completely different for two THG systems. From Fig. 6(c), one can see that most of the hot spot is localized in the silica shell for the core-shell system. However, most hot spots exist in the air for the gap system. Only a little spreads across the Au surface. The third-order nonlinear susceptibility of Au outclasses that of silica.

3. Conclusion

In conclusion, we have presented a novel THG design by using a gain-assisted Au NR, which, owing to its NP morphology, has flexibility that is well-suited for actual applications. As such, this Au NR can be fabricated simply, without the need for high-resolution semiconductor techniques, and contributes to a super-high efficiency THG. By using FDTD simulation and Fourier analysis, we successfully separated the third harmonics from the total fields of the excitation laser. Results revealed the outer gain layer has an optimal gain coefficient, where an $\sim$239.7-fold third harmonics can be obtained compared to those using the same structure without the gain coefficient. The results also show that the THG enhancement of the gain-assisted Au nanorod with a critical gain coefficient is one to two orders of magnitude greater than the highest values reported for gap THG systems.

Acknowledgment

J. Song and J. Xian contributed equally to this work.

References

[1] Q. Xu *et al.*, "Aluminum plasmonic nanoparticles enhanced dye sensitized solar cells," *Opt. Exp.*, vol. 22, no. 102, pp. A301–A310, Mar. 2014.
[2] C. X. Wang *et al.*, "A galvanic replacement route to prepare strongly fluorescent and highly stable gold nanodots for cellular imaging," *Small*, vol. 9, no. 3, pp. 413–420, Feb. 2013.
[3] T. Shegai, B. Brian, V. D. Miljković, and M. Käll, "Angular distribution of surface-enhanced Raman scattering from individual Au nanoparticle aggregates," *ACS Nano*, vol. 5 no. 3, pp. 2036–2041, Mar. 2011.
[4] K. D. Lu, C. B. He, and W. B. Lin, "Nanoscale metal-organic framework for highly effective photodynamic therapy of resistant head and neck cancer," *J. Amer. Chem. Soc.*, vol. 136, no. 48, pp. 16712–16715, Dec. 2014.
[5] I. N. M. Wijeratne, N. Kejalakshmy, B. M. A. Rahman, and K. T. V. Grattan, "Rigorous full-vectorial beam propagation analysis of second-harmonic generation in zinc oxide waveguides," *IEEE Photon. J.*, vol. 5, no. 2, Apr. 2013, Art. ID. 6100112.
[6] M. K. Vanbel *et al.*, "Tunneling of holes is observed by second-harmonic generation," *Appl. Phys. Lett.*, vol. 102, no. 8, Feb. 2013, Art. ID. 082104.
[7] K. Thyagarajan, S. Rivier, A. Lovera, and O. J. F. Martin, "Enhanced second-harmonic generation from double resonant plasmonic antennae," *Opt. Exp.*, vol. 20, no. 12, pp. 12860–12865, Jun. 2012.
[8] R. Czaplicki *et al.*, "Enhancement of second-harmonic generation from metal nanoparticles by passive elements," *Phys. Rev. Lett.*, vol. 110, no. 9, Feb. 2013, Art. ID. 093902.
[9] M. A. Gouveia *et al.*, "Second harmonic generation and enhancement in microfibers and loop resonators," *Appl. Phys. Lett.*, vol. 102, no. 20, May 2013, Art. ID. 201120.
[10] K. Konishi *et al.*, "Polarization-controlled circular second-harmonic generation from metal hole arrays with threefold rotational symmetry," *Phys. Rev. Lett.*, vol. 112, no. 13, Apr. 2014, Art. ID. 135502.
[11] M. L. Ren, W. J. Liu, C. O. Aspetti, L. X. Sun, and R. Agarwal, "Polarization-controlled circular second-harmonic generation from metal hole arrays with threefold rotational symmetry," *Nat. Commun.*, vol. 5, p. 5432, Nov. 2014.
[12] K. Thyagarajan, J. Butet, and O. J. F. Martin, "Augmenting second harmonic generation using Fano resonances in plasmonic systems," *Nano Lett.*, vol. 13, no. 4, pp. 1847–1851, Apr. 2013.
[13] G. F. Walsh and L. D. Negro, "Enhanced second harmonic generation by photonic-plasmonic Fano-type coupling in nanoplasmonic arrays," *Nano Lett.*, vol. 13, no. 7, pp. 3111–3117, Jul. 2013.

[14] G. Grinblat *et al.*, "High-efficiency second harmonic generation from a single hybrid ZnO nanowire/Au plasmonic nano-oligomer," *Nano Lett.*, vol. 14, no. 11, pp. 6660–6665, Nov. 2014.
[15] T. Wu, Y. Sun, X. Shao, P. P. Shum, and T. Huang, "Highly efficient phase-matched third harmonic generation from mid-IR to near-IR regions using an asymmetric plasmonic slot waveguide," *IEEE Photon. J.*, vol. 6, no. 5, Oct. 2014, Art. ID. 4801709.
[16] M. Hentschel, T. Utikal, H. Giessen, and M. Lippitz, "Quantitative modeling of the third harmonic emission spectrum of plasmonic nanoantennas," *Nano Lett.*, vol. 12, no. 7, pp. 3778–3782, Jul. 2012.
[17] B. Metzger, T. Schumacher, M. Hentschel, M. Lippitz, and H. Giessen, "Third harmonic mechanism in complex plasmonic Fano structures," *ACS Photon.*, vol. 1, no. 6, pp. 471–476, Jun. 2014.
[18] K. Li, X. F. Li, D. Y. Lei, S. L. Wu, and Y. H. Zhan, "Plasmon gap mode-assisted third-harmonic generation from metal film-coupled nanowires," *Appl. Phys. Lett.*, vol. 104, no. 26, Apr. 2014, Art. ID. 261105.
[19] H. Aouani, M. Rahmani, M. Navarro-Cia, and S. A. Maier, "Third-harmonic-upconversion enhancement from a single semiconductor nanoparticle coupled to a plasmonic antenna," *Nature Nanotechnol.*, vol. 9, no. 4, pp. 290–294, Apr. 2014.
[20] T. Huang *et al.*, "Efficient third-harmonic generation from 2 μm in asymmetric plasmonic slot waveguide," *IEEE Photon. J.*, vol. 6, no. 3, Jun. 2014, Art. ID. 4800607.
[21] C. Wang *et al.*, "Nondegenerate four-wave mixing in a dual-mode injection-locked InAs/InP(100) nanostructure laser," *IEEE Photon. J.*, vol. 6, no. 1, Feb. 2014, Art. ID. 1500408.
[22] A. Yi *et al.*, "Polarization-insensitive and receiver-sensitivity-gain format conversion for PDM signals based on dual-orthogonal-pump four-wave mixing in highly nonlinear fiber," *IEEE Photon. J.*, vol. 7, no. 1, Feb. 2015, Art. ID. 7200606.
[23] M. R. Dizaji, I. A. Kostko, B. Shia, C. L. Callender, and P. Dumais, "Reconfigurable time slot interchange based on four-wave mixing and a programmable planar lightwave circuit," *IEEE Photon. J.*, vol. 6, no. 5, Oct. 2014, Art. ID. 7902907.
[24] X. Y. Huang, S. Y. Han, W. Huang, and X. G. Liu, "Enhancing solar cell efficiency: The search for luminescent materials as spectral converters," *Chem. Soc. Rev.*, vol. 42, no. 1, pp. 173–201, Jan. 2013.
[25] R. Weissleder, "A clearer vision for in vivo imaging," *Nat. Biotechnol.*, vol. 19, no. 4, pp. 316–317, Apr. 2001.
[26] A. V. Kachynski *et al.*, "Photodynamic therapy by in situ nonlinear photon conversion," *Nat. Photon.*, vol. 8, no. 6, pp. 455–461, Jun. 2014.
[27] J. Butet, K. Thyagarajan, and O. J. F. Martin, "Ultrasensitive optical shape characterization of gold nanoantennas using second harmonic generation," *Nano Lett.*, vol. 13, no. 4, pp. 1787–1792, Apr. 2013.
[28] Z.-Y. Li and Y. Xia, "Metal nanoparticles with gain toward single-molecule detection by surface-enhanced Raman scattering," *Nano Lett.*, vol. 10, no. 1, pp. 243–249, Jan. 2010.
[29] J. Xian, L. Chen, H. Niu, J. Qu, and J. Song, "Significant field enhancements in an individual silver nanoparticle near a substrate covered with a thin gain film," *Nanoscale*, vol. 6, no. 22, pp. 13–994–14–001, Nov. 2014.
[30] P. B. Johnson and R. W. Christy, "Optical constants of noble metals," *Phys. Rev. B, Condens. Matter*, vol. 6, no. 12, pp. 4370–4379, Dec. 1972.
[31] M. A. Noginov *et al.*, "Demonstration of a spaser-based nanolaser," *Nature*, vol. 460, no. 7259, pp. 1110–1112, Aug. 2009.
[32] S.-Y. Liu *et al.*, "Simultaneous excitation and emission enhancement of fluorescence assisted by double plasmon modes of gold nanorods," *J. Phys. Chem. C*, vol. 117, no. 20, pp. 10636–10642, May 2013.
[33] S. Charan *et al.*, "Development of chitosan oligosaccharide-modified gold nanorods for in vivo targeted delivery and noninvasive imaging by NIR irradiation," *Bioconjugate Chem.*, vol. 23, no. 11, pp. 2173–2182, Nov. 2012.
[34] S.-Y. Liu, J. Li, F. Zhou, L. Gan, and Z.-Y. Li, "Efficient surface plasmon amplification from gain-assisted gold nanorods," *Opt. Lett.*, vol. 36, no. 7, pp. 1296–1298, Apr. 2011.
[35] N. Ueda *et al.*, "Third-order nonlinear optical susceptibilities of electroconductive oxide thin films," *Appl. Phys. Lett.*, vol. 59, no. 5, pp. 502–503, Jul. 1991.
[36] H. Kollmann *et al.*, "Toward plasmonics with nanometer precision: Nonlinear optics of helium-ion milled gold nanoantennas," *Nano Lett.*, vol. 14, no. 8, pp. 4778–4784, Aug. 2014.